ELSEVIER

Journal of Structural Geology 30 (2008) 257–272

JOURNAL OF STRUCTURAL GEOLOGY

www.elsevier.com/locate/jsg

The 3D geometry of small-scale relay zones between normal faults in soft sediments

M.B. Kristensen [a,b,c,*], C.J. Childs [b], J.A. Korstgård [a]

[a] *Department of Earth Sciences, University of Aarhus, Høegh-Guldbergs Gade 2, DK-8000 Aarhus C, Denmark*
[b] *Fault Analysis Group, UCD School of Geological Sciences, University College Dublin, Belfield, Dublin 4, Ireland*
[c] *Shell U.K. Limited, 1 Altens Farm Road, Nigg, Aberdeen AB12 3FY, United Kingdom*

Received 12 September 2006; received in revised form 12 November 2007; accepted 13 November 2007
Available online 17 November 2007

Abstract

Serial cross-sections of faults within soft sediments of Miocene age, on the East coast of Denmark, were collated to provide 3D data sets with which to study the geometry of minor faults (displacements < 10 cm). From the wide variety of geometrical complexities displayed by these faults, many due to mutually cross-cutting relationships between opposed dipping faults, we present relatively simple structures considered to demonstrate stages in the evolution of relay zones between overlapping fault segments. The structures described are: (1) initial embayments in fault tip-lines, (2) established relay zones displaying transfer of displacement between overlapping fault segments, (3) breached relay zones, and (4) fault bound lenses. An individual relay zone may display more than one of these structures along its length and relay zones that are intact on one cross-section may be breached along strike on another. Examples of relay zones that are isolated from the fault tip-line and are effectively holes within a continuous fault are also observed. The observed relay zones breach by propagation of the initial parent fault through the relay zone rather than by the formation of a new breaching fault.

Keywords: Normal faults; Segmentation; Fault propagation; Relay zone; Fault linkage

1. Introduction

Faults are rarely simple planar structures, but rather form segmented arrays both in map view and in cross-section (e.g. Larsen, 1988; Peacock and Sanderson, 1991, 1994; Huggins et al., 1995; Childs et al., 1995, 1996a; Marchal et al., 1998, 2003; Peacock, 2002; Walsh et al., 2003). The rock volumes between adjacent segments of a fault array are zones of high strain that accommodate the transfer of displacement between segments; these zones are referred to as relay zones (Childs et al., 1995). As displacement accumulates on a segmented fault array, the strains within the relay zones increase until the relay zones are breached by the formation of a through-going fault (Ramsay and Huber, 1983; Peacock and Sanderson, 1991; Childs et al., 1995). Fault segmentation and relay zone breaching occur on a wide range of scales and are two of the main processes controlling the geometrical evolution of faults (Huggins et al., 1995; Morley and Burhannudinnur, 1997; Burhannudinnur and Morley, 1997; Marchal et al., 1998, 2003; Walsh et al., 2003; Kristensen, 2005).

Segmented fault arrays can form in two ways, by the coincidental alignment of initially isolated faults or by the initiation of fault segments as elements within a larger structure. In the first case, the initially isolated faults propagate towards one another until their deformation fields overlap and relay zones transferring displacement are established (Peacock and Sanderson, 1991; Cartwright et al., 1995; Mansfield and Cartwright, 2001; Peacock, 2002). In the second case, fault segments initiate within a narrow zone as parts of a coherent array where transfer of displacement between segments occurs from the outset (Childs et al., 1995; Walsh et al., 2003). Such coherent arrays can comprise segments that are unconnected

* Corresponding author. Shell U.K. Limited, 1 Altens Farm Road, Nigg, Aberdeen, AB12 3FY, United Kingdom.
E-mail address: mette.bundgaard@geo.au.dk (M.B. Kristensen).

0191-8141/$ - see front matter © 2007 Elsevier Ltd. All rights reserved.
doi:10.1016/j.jsg.2007.11.003

in three dimensions or a series of fault lobes connected to a continuous fault surface; the segmented faults described here are all interpreted to have formed as coherent arrays. Analysis of seismic reflection data sets from areas of normal faulting (Childs et al., 1995; Rowan et al., 1998) and sandbox models (e.g. Marchal et al., 2003) have shown that segmented arrays of normal faults mapped on a horizon are commonly connected above or below the mapped level. There are, however, very few accounts of seismically mapped normal faults that are segmented in cross-sectional view (but see Walsh et al., 1999; Kattenhorn and Pollard, 2001). In this paper we present examples of relay zones seen in cross-section, both intact and breached, where the geometry in three dimensions is well constrained from serial sections through small normal faults in soft sediments.

Uncemented, high porosity sediments have lower shear modulus and more readily accommodate volumetric strains than sandstones, for example, so that faults within them have higher displacement gradients than faults in sandstones (Wibberley et al., 1999). The overlap lengths of intact relay zones between fault segments of a given throw are therefore smaller, and more readily studied, in high porosity sediments than in stiffer, lithified sediments. The faults studied here are in sediments comprising finely interbedded sands and silts (Kristensen, 2005), which allow very accurate mapping of fault surfaces and displacements, providing an opportunity to study the 3D geometry of segmented faults at a resolution that is unattainable using other types of data.

The relay zone structures presented are described with reference to a four-stage model of relay zone evolution (Fig. 1) based on previous studies (Peacock and Sanderson, 1994; Huggins et al., 1995; Childs et al., 1996b, 1997; Hus et al., 2005). In this model, local retardation of a propagating fault tip-line results in the bifurcation of the fault surface (Stage 1), creating a zone of overlap and a relay zone between two connected fault lobes (Stage 2). As displacement increases, the relay zone becomes breached to form a through-going fault (Stage 3) and with further displacement the two fault-lobes link to form a fault bounded lens (Stage 4). Fig. 1 illustrates the model for a laterally propagating fault tip-line (i.e. propagation parallel to bedding) but could also be illustrated for a vertically propagating fault.

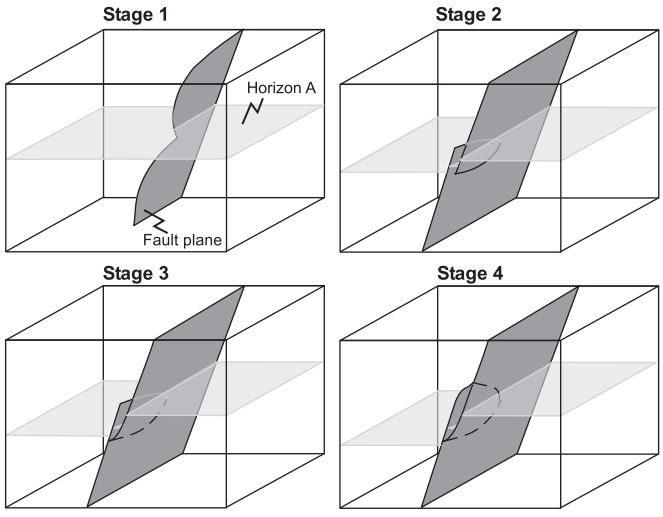

Fig. 1. Conceptual model for the evolution of relay zones illustrated for a normal fault surface (dark shading) propagating laterally through a rock volume, from the back to the front of the block diagram. A horizontal bedding surface within the rock volume is shown (light shading). The propagation of the tip-line is locally retarded causing an embayment in the fault surface and bifurcation of the surface into two fault-lobes (Stage 1). In Stage 2, the fault surface has propagated through the rock volume and the fault lobes have propagated along strike and out of plane from one another, to form a contractional relay zone. Increased fault displacement causes increasingly higher strains within the relay zone, which eventually breaches with the formation of a through-going fault surface (Stage 3). Further increase in fault displacement may result in the formation of a lens of fault bounded rock (Stage 4). Modified from Childs et al. (1997).

1.1. Terminology

In this paper we distinguish three different types of relay zone depending on the nature of the strains within them (Fig. 2; Walsh et al., 1999). Relay zones between normal fault segments, which overlap on vertical cross-sections, are referred to as 'contractional' or 'extensional' depending on the sense of overlap of the fault segments and the nature of the volumetric strain required to transfer displacement between them. Relay zones between normal faults, which overlap along strike, are referred to as 'neutral' as no volumetric strains are required to transfer displacement between the relay bounding faults. Many relay zones described in this manuscript do not conform to these simple end-member types but are oblique, displaying relay zone characteristics both in cross-section and in map view.

2. Study area

The study area is situated on a recently exposed coastal section through finely (mm–cm) interbedded Miocene, fine sands, silts and clays at Jensgaard on the East coast of Jutland, Denmark (Fig. 3, inset) (Rasmussen and Dybkjær, 2005). The faulted outcrop is a ~3 m high, 50 m long, approximately N–S striking coastal exposure. The majority of the faults strike E–W and dip both to the S and N, with dips ranging from 30° to 70°. The exposed faults have throws up to 15 cm and are commonly layer-bound, tipping-out in underlying and overlying thin (<10 cm) clay-rich intervals. Due to the high fault density (up to ~15 faults/m) the majority of faults cross-cut opposed dipping and synchronous faults to form conjugate structures. Shallow dipping normal faults with displacements of up to 15 cm crosscut the clay intervals and postdate the steeper faults. The faulted section is directly overlain by unfaulted glacial till. The base of the till is composed of reworked Miocene sediments. In contrast, the upper part of the till (which resembles those more commonly observed in Denmark) is more sandy with a variety of glacially transported crystalline clasts. The exposure is truncated to the south by a sequence of dark, most likely lagoonal, muds. The contact is sharp and marked by a 2 cm wide zone of sheared sediment suggesting that it is a faulted contact. Towards the northern end of the exposure, the Miocene sediments are intruded by a mud diapir (ca. 6 m wide). Bedding in the sediments

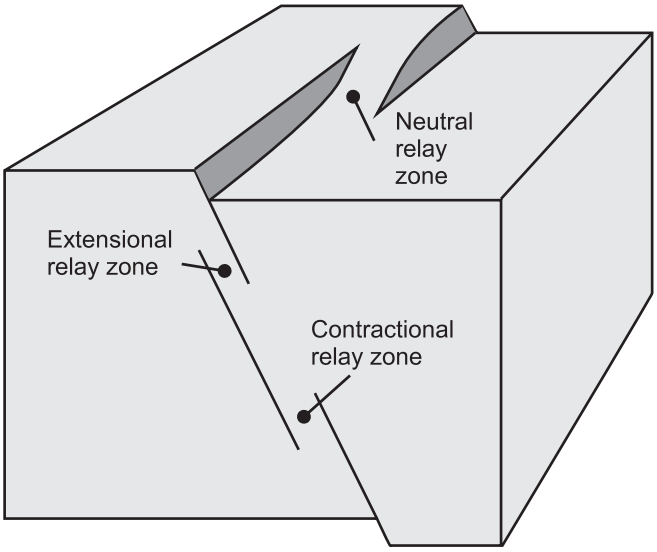

Fig. 2. Block diagram illustrating the three end-member types of relay zone distinguished in this paper. The tip-lines of the fault segments bounding the extensional and contractional relay zones are normal to the front face of the block diagram. The tip-lines of the segments bounding the neutral relay zone are parallel to the fault slip vector.

adjacent to the diapir dips steeply away from the diapir and the faults are rotated with bedding indicating that faulting occurred prior to the deformation associated with emplacement of the diapir. The maximum burial depth of the faulted sediments is estimated to be ca. 300–500 m based on the thicknesses of the overlying sections elsewhere (Erik S. Rasmussen, 2005, personal communication).

The precise cause of faulting is unknown. Several different fault trigger mechanisms are possible: (i) differential compaction of underlying mud and associated diapirism; (ii) faulting associated with larger scale tectonically driven Miocene block faulting, as observed on a N–S 2D high resolution seismic line shot in the bay offshore from the study area (Holger Lykke-Andersen, unpublished data); and (iii) faulting due to glacial tectonics (Rasmussen and Dybkjær, 2005).

3. Methods

Three-dimensional data sets for four faulted sediment volumes were made by serial sectioning the vertical cliffs of soft Miocene sediments at Jensgaard on the East coast of Denmark. Each section was photographed normal to the outcrop and the photographs were collated to recreate the faulted 3D sedimentary volume. The dimensions of individual 2D sections were between 50 cm and 90 cm wide and 40–60 cm high. The sections were spaced at 0.5–2.5 cm intervals and excavated to depths up to 29 cm into the cliff. To minimize distortion on the photographs, the orientations of the serial sections were kept constant by monitoring their strike and dip. Where outcrop topography permitted, the camera was positioned on a fixed stage, otherwise the camera was hand-held.

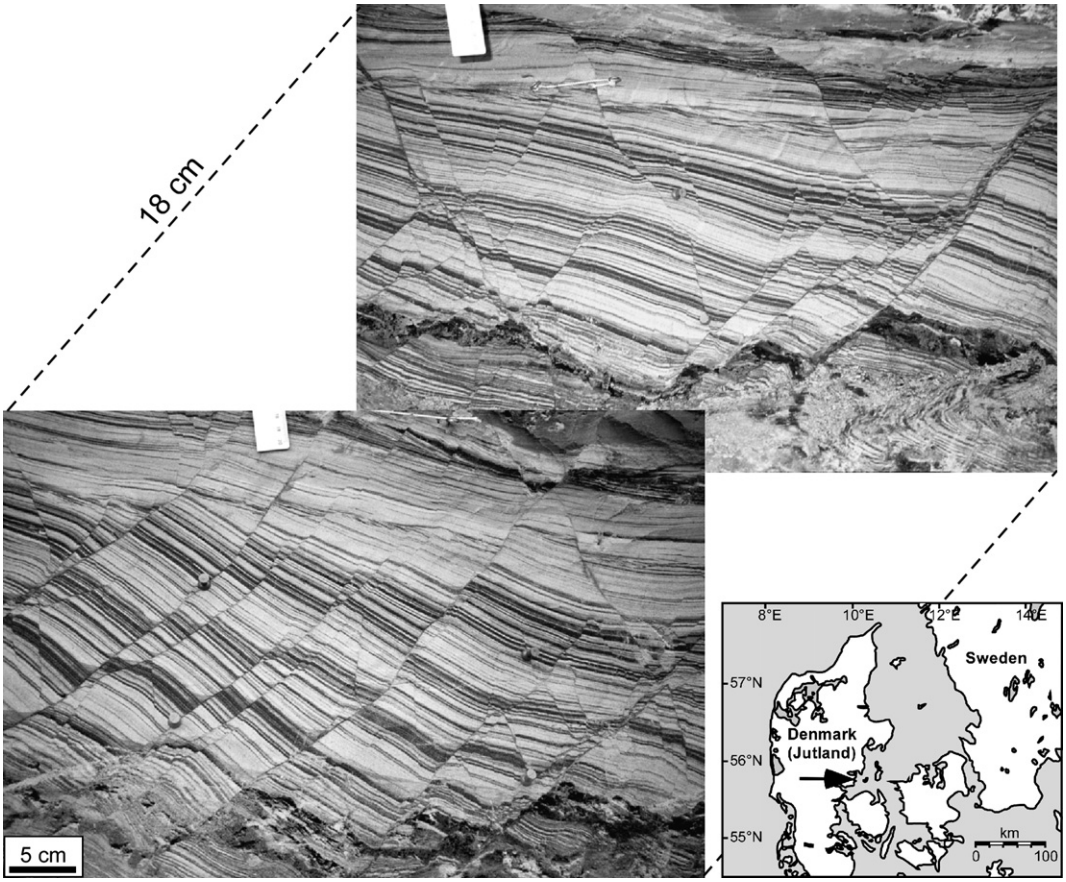

Fig. 3. Two serial sections from one of the 3D surveys cut through faulted soft sediments at Lillebælt, Jensgaard, on the East coast of Denmark (map insert with arrow).

Laser pointers were used to create fixed points on consecutive sections, providing a guide in reconstruction and alignment of the serial sections. These were used in conjunction with the sedimentary layering to reconstruct and align the scaled photographs. Photographic distortion, due to minor variations in camera angle and slightly uneven outcrop sections, and uncertainty in relative scaling and positioning of the sections have introduced some errors to the end results, but we estimate that the relative positions of faults on successive sections are accurate to within 1 mm. Throw measurement errors on individual photographic sections are determined by digitizing accuracy which is significantly less than 1 mm.

The photographic sections were imported into a seismic interpretation package and the faults and horizons were interpreted using the same methods used in interpreting 3D seismic surveys. The layering of fine-grained sands, silts and illite/kaolinite rich clays makes these tidal sediments ideal for detailed displacement analysis along faults in cross-section and along strike as individual horizons are continuous across the scale of the structures investigated.

4. General fault characteristics in 2D

The faults studied have throws of up to 15 cm. Low displacement faults (<1 cm) are commonly single stranded, while faults with higher displacements (ca. 10 cm) consist of multiple fault strands along much of their trace lengths (Fig. 3). Fault tips are commonly observed on cross-sections. Some faults terminate as open monoclines, while others terminate at discrete tip-points with no associated normal drag. A variety of structures are observed in cross-sections such as fault relay zones, splays and lenses. Both contractional and extensional relay zones occur, and both types of structure may be seen along a single fault trace. Faults splay both down- and up-dip with splays occurring both on the hanging wall and footwall side of the parent fault. Splays are observed both close to the tip of the parent faults and along the fault trace. The geometry at branch points between fault splays is variable. Fault splays may link to the parent fault at very low angles, while other fault traces are curved towards the parent fault to intersect at high angles (up to 60°). Fault bounded lenses of variable sizes and shapes are observed along fault traces. Similar to the fault splays, some lens bounding fault traces link at an acute angle, while others are deflected towards the branch point with the parent fault, to intersect at high angles. Lenses may contain slivers of intact host sediments or may be faulted internally. Burhannudinnur and Morley (1997) describe very similar fault splay and lens geometries in outcrops of faults in poorly lithified sandstone and shale. In the following sections we describe in detail the 3D fault geometries these typical fault trace geometries represent.

5. Field examples of fault growth stages

The internal structure of faults with up to tens of centimeter displacement is generally complex, with displacement distributed on multiple anastomosing and rejoining splays. In this study we are not concerned with these structures, but rather we present simple structures on low displacement faults, to illustrate the different 3D geometries that we interpret as stages in fault propagation and relay zone evolution in these sediments. The complex internal structures of larger displacement faults are interpreted to be the result of the repeated action of propagation related processes and processes active after a through-going fault has formed, e.g. asperity removal. At outcrop, the faults in these sediments are relatively discrete discontinuities, but can be seen to be narrow shear zones when viewed under the microscope. The fine laminations allow detailed mapping of fault geometry and displacement distribution in three dimensions. While the individual structures presented (relay zones, fault bound lenses, etc.) are contained entirely within the survey from which they were derived, the faults on which they occur generally extend outside the data volume.

5.1. Stage 1 – bifurcation

Continuous fault surfaces that bifurcate to form fault lobes towards their tip regions (Stage 1, Fig. 1) are commonly observed in these faults and an example of a fault surface that displays this geometry is shown in Fig. 4. The fault appears as two separate and isolated fault segments in cross-sections close to its lateral termination (Fig. 4A, cross-section at 0 cm, Fig. 4B). On cross-sections from 0 cm to 5.5 cm the tips of the two segments become progressively closer to one another forming an underlapping contractional relay zone. Further along strike the segments merge (Fig. 4A, cross-section at 6 cm and Fig. 4B) to become one continuous fault surface with a contractional bend within a sand dominated interval (Fig. 4A, arrow on cross-section at 6 cm). Throw profiles on cross-sections from 0 cm to 5.5 cm show that the throw on the two fault-lobes is similar (Fig. 4C). Between the fault lobes the throw is zero and this throw deficit is accommodated by continuous deformation, i.e. monoclinal folding between the fault tips (Fig. 4A cross-section at 0 cm). This monocline has a half-wavelength of ~2 cm and an amplitude equal to the throw on the two faults, and is interpreted to effect the transfer of displacement between the fault lobes. The low throw on the continuous fault on the 6 cm cross-section is due to the presence of monoclinal folding on either side of the continuous fault trace. This folding is interpreted to have developed between initially underlapping fault segments, as shown by the present day structure of the cross-section at 0 cm, which was subsequently bypassed when the fault segments linked. The overall structure is interpreted to have formed by bifurcation during lateral propagation of the fault tip-line (from the area of relatively high displacement on the right of Fig. 4B towards the tip-line on the left; Fig. 1, Stage 1), with linkage between the fault lobes occurring following a period of displacement transfer by monoclinal folding. The point at which bifurcation initially occurred is further along strike of the section at 6 cm.

Fig. 5 shows a fault surface that bifurcates along strike to form four discrete fault segments near the tip of the fault.

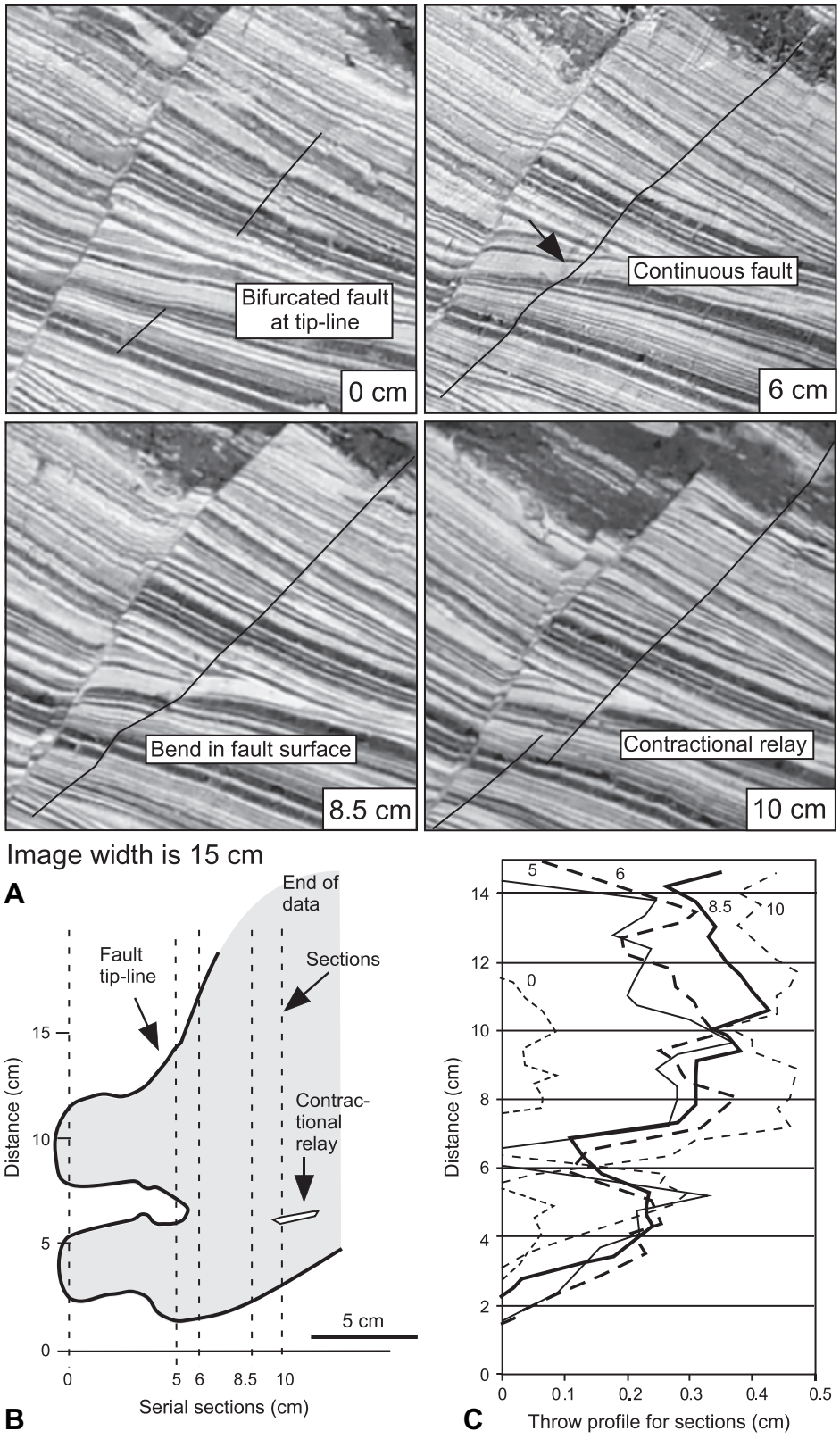

Fig. 4. An example of a part of a fault surface with an embayment in the lateral tip-line and a contractional relay zone contained within the fault surface. (A) Four selected cross-sections through the fault surface located at 0 cm, 6 cm, 8.5 cm and 10 cm behind the original outcrop face. The arrow on the cross-section at 6 cm indicates the location of the contractional bend on the fault trace discussed in the text. (B) Outline of the fault surface (shaded) projected onto a vertical plane parallel to fault strike and viewed from the hanging wall of the fault. The fault tip-line is shown (heavy line) and the right hand margin of the fault surface is at the end of the available data. The shape of the fault surface is constrained by 18 vertical sections and the relative locations of the four sections in A are shown. (C) Profiles of fault throw for cross-sections at 0 cm, 5 cm, 6 cm, 8.5 cm and 10 cm shown in B.

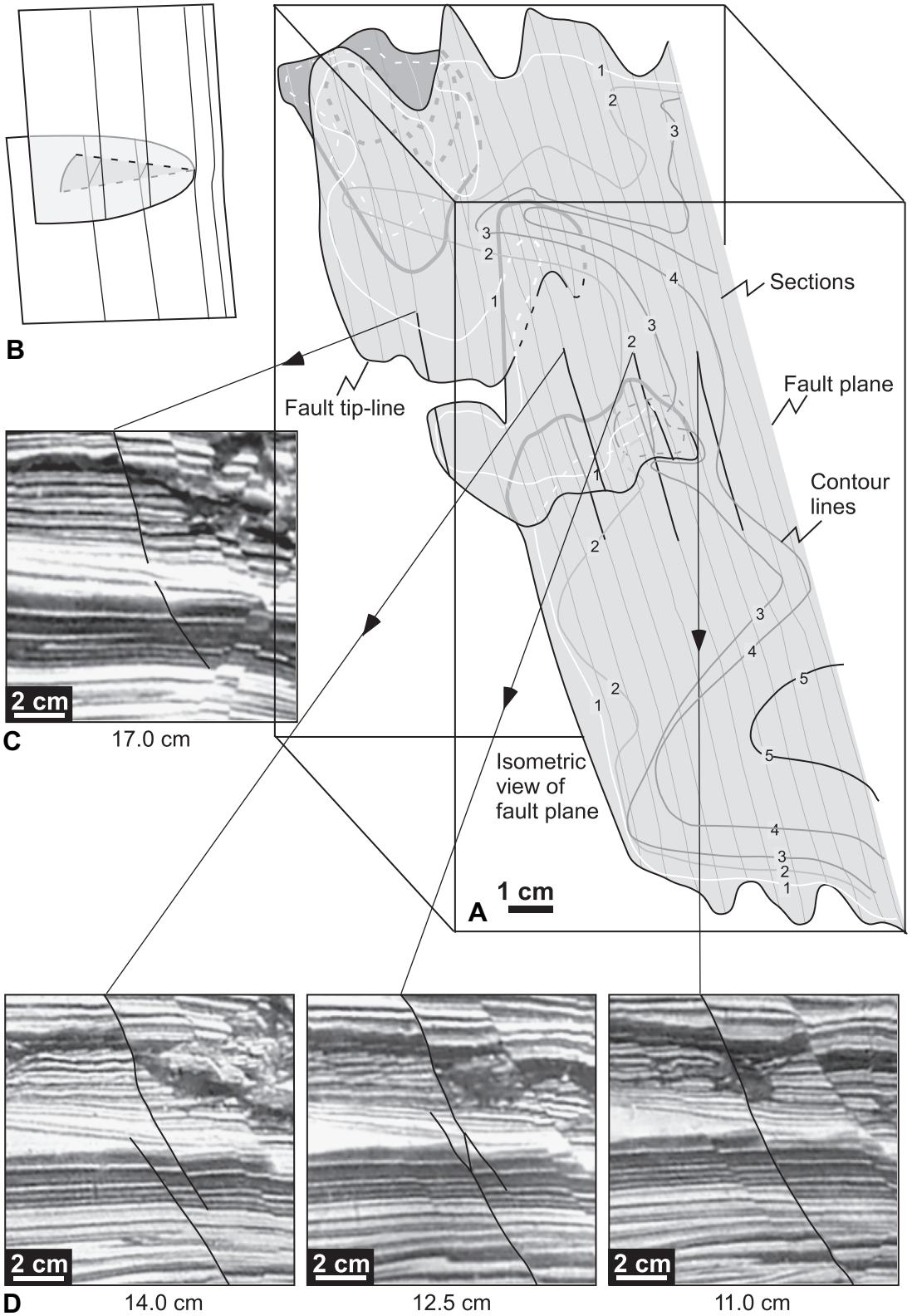

Fig. 5. (A) Isometric view of the lateral margin of a fault surface, which is bifurcated into four separate lobes. Fault tip-lines are heavy lines, shown grey where obscured by other fault segments. Dashed black lines are branch-lines. The fault surface is contoured for throw (mm) and contours are dashed where obscured. The thin grey lines show the fault geometry on each of the 17 sections used in defining the fault surface geometry and displacement distribution. (B) Schematic insert illustrating the interpreted 3D geometry of the structure illustrated in (D) on cross-sections 11–14 cm. Thin lines indicate fault trace geometries. (C) Part of the cross-section at 17.0 cm. (D) Parts of cross-sections at 14.0 cm, 12.5 cm and 11.0 cm at the locations shown in (A).

Two of these segments (cross-section at 17 cm in Fig. 5C) display a similar geometry to that shown in Fig. 4A, B, with discrete offset of horizons along two co-planar fault segments separated by an area of fault related drag. Again, this structure is interpreted to have formed during lateral tip propagation (right to left on Fig. 5A); the fault is assumed to have propagated from the area of relatively high displacement, on the right in Fig. 5A, towards the present day tip-line. In this case the two fault-lobes overlap along strike to form an extensional relay zone closer to the continuous parent fault (see fault cross-sectional traces on Fig. 5A). The remaining details of Figs. 4 and 5 are discussed in Section 5.2.

5.2. Stage 2 – relay zone

Following bifurcation of a fault surface, in the second stage of relay zone evolution (Fig. 1), two lobes of a bifurcated fault surface overlap to form a relay zone. Depending on the relative positions of the overlapping faults, relay zones may be extensional, contractional or neutral (Fig. 2). Here we present examples of extensional and contractional relay zones.

Fig. 5A shows a 3D fault surface map for a segmented normal fault array. Displacement contours on the fault surface illustrate the complex displacement distribution associated with segmented faults. The mapped portion of the fault surface contains two extensional relay zones, in addition to a footwall splay that links to the parent fault along a vertical branch-line (Fig. 5A upper left). The 3D geometry of the lower of the two extensional relay zones is illustrated with three cross-sections (Fig. 5D) and shown schematically in Fig. 5B. A single continuous fault surface (cross-section at 11.0 cm) bifurcates along strike and forms two overlapping fault lobes with a connecting fault between the lobes (cross-section at 12.5 cm). Further along strike (cross-section at 14.0 cm) the connecting fault is absent and the two fault-lobes form an intact extensional relay zone. Transfer of displacement between the overlapping fault segments occurs by fault parallel extension of the sediment volume within the relay zone. The magnitude of this extension is given by the ratio between the fault displacements immediately above or below the relay zone and the length of overlap between the relay bounding fault traces, which for the cross-section at 14 cm is 0.1. This structure is again interpreted to have formed by bifurcation of a laterally propagating tip-line. Between 11.0 cm and 12.5 cm there is an extensional bend on the fault surface (shown schematically on the right hand side of Fig. 5B). This bend can be interpreted as either (1) resulting from tip-to-tip linkage of two initially underlapping fault lobes where the initial relay geometry is not recorded as bypassed splays or (2) a deflection of the fault surface during lateral fault propagation prior to fault bifurcation further along strike.

An example of a contractional relay zone is illustrated in Fig. 6. Cross-sections through the centre of the relay zone show two overlapping fault segments (Fig. 6B). The location of these is highlighted in Fig. 6A, which shows the interpreted fault lobes in three dimensions. In contrast to the previous structures, the fault lobes link along strike in *both* directions so that the relay zone is effectively a gap in an otherwise continuous fault surface (Fig. 6A, D). Transfer of displacement between the overlapping fault lobes is demonstrated by the high throw gradients on the overlapping segments and their complementary displacement variations, which yield a relatively smooth aggregate throw profile (Fig. 6C). Departure from a completely smooth aggregate profile is due to normal drag of the beds, and to a minor antithetic fault between the overlapping segments (Fig. 6B). In three dimensions the transfer of displacement between the overlapping lobes is reflected in displacement contours (Fig. 5A), which loop between the two lobes, either continuously around the outside of the relay zone (5 mm contour) or via the branch-lines at which the two lobes connect. Transfer of displacement between the fault lobes requires contractional strains within the relay zone. These strains are at a minimum of 0.17 (17% shortening) at the centre of the relay zone (Fig. 6B) and increase towards the margins of the relay zone where the length of overlap of the two lobes decreases and displacement gradients are higher, as seen by the bunching of contours on the fault surface map (Fig. 6A).

The fault separation is a maximum ($\sim$9 mm) at the centre of the relay zone, decreasing along strike in both directions. Tip-lines bounding the fault lobes at the centre of the relay zone are replaced along strike by branch-lines along which the lobes are connected. At the left-hand side of the structure (Fig. 6A), the overlapping fault segments link to form a fault bounded lens in cross-section giving way to a continuous and straight fault further along strike. Linkage at the right hand side of the relay zone alternates from the hanging wall segment linking to the footwall, to the footwall segment linking to the hanging wall segment, before the segments merge to form a continuous, planar fault surface on the cross-sections thereafter.

The tip-line loop, which outlines the gap in the fault surface illustrated in Fig. 6, is interpreted to have originated as an embayment of the tip-line bounding the fault surface, resulting in two fault-lobes that rejoined to leave a hole on the fault in their wake. There is no clear geometrical feature on the fault surface that indicates the line along which the two lobes coalesced and neither is there any clear indication of the direction of fault propagation, however, by analogy with the structures in Figs. 4 and 5, lateral propagation is favoured. The alternative explanation, i.e. the structure is the result of vertical fault propagation, would require that the fault tip-line was pinned at two points, i.e. the sites of the points of linkage between the lobes, and that the lobes coalesced along a line that somewhere intersects the tip-line loop, for which there is no evidence. Lateral propagation provides the simpler explanation of the observed structure with one end of the relay zone representing the point of bifurcation and the other the point of linkage, while vertical propagation requires two bifurcation points and a line of linkage, which cannot be identified.

A similar structure occurs on the fault surface illustrated in Fig. 4. Along fault strike from the lateral fault termination and bifurcated tip-line described previously, this fault surface has an intact contractional relay zone, preserving a ‘‘gap’’ within

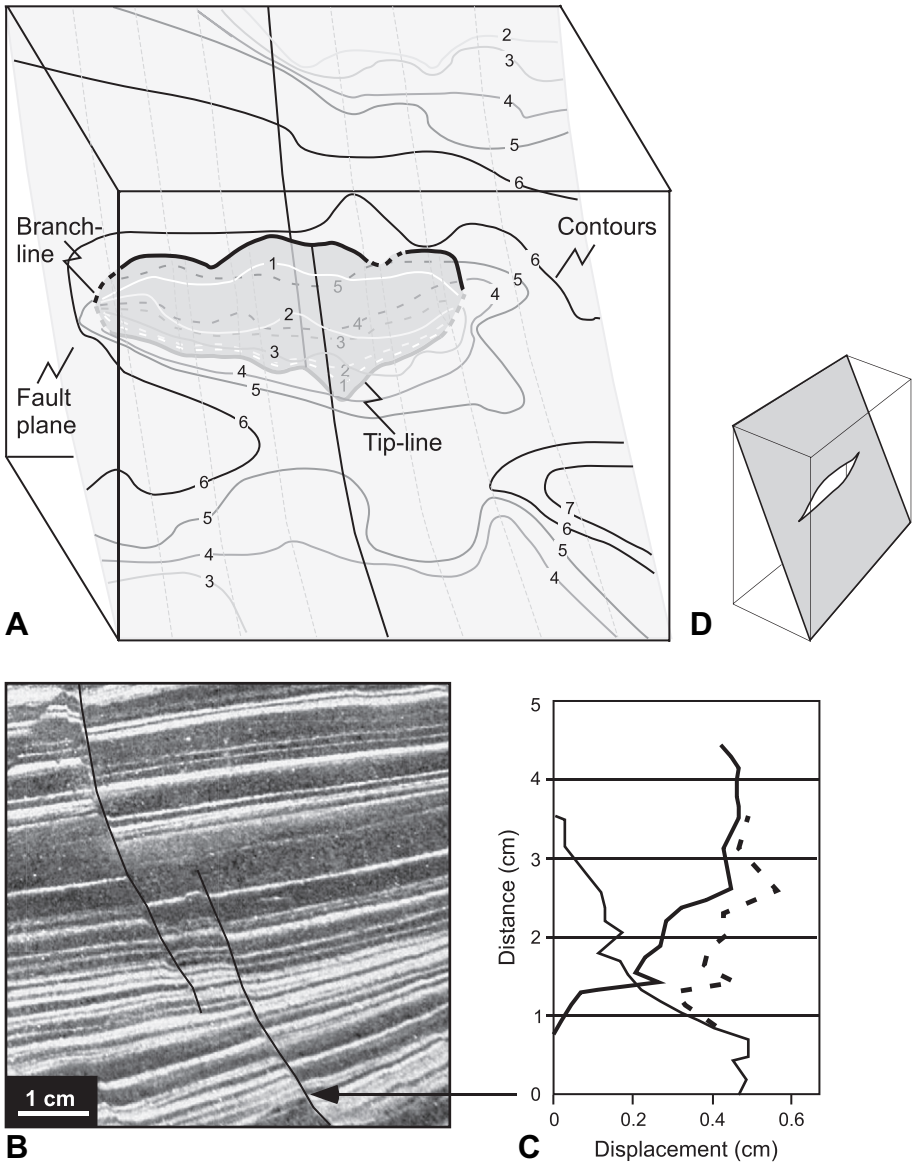

Fig. 6. (A) Map of part of a fault surface with a contractional relay zone. Darker shading indicates areas where the two relay bounding fault segments overlap. Fault tip-lines are shown with heavy lines (grey in the footwall) and branch-lines are heavy dashed lines. The fault trace geometry on alternate cross-sections is shown in thin, grey, dotted lines. The fault surface is contoured for displacement (mm) and contours are dashed in the footwall. (B) Cross-section through the relay zone on the line highlighted in black in (B). (C) Displacement profiles for the two fault trace segments in (B), and their aggregate displacement (dashed line). The *Y*-axis is vertical distance and displacement on the fault segments is aggregated on a horizon basis. (D) Schematic illustration of the 3D geometry of this structure.

the otherwise continuous fault surface (Fig. 4A, cross-section at 10 cm). The cross-section at 8.5 cm (Fig. 4A) shows a bend in the continuous fault surface at the level of the contractional overlap seen on the cross-section at 10 cm. The two overlapping fault surfaces are again interpreted to have formed by lateral propagation and along-strike coalescence of two fault-lobes.

5.3. Stage 3 – breaching

In the third stage of relay zone evolution (Fig. 1), fault segments become linked and the relay zone separating them is breached. Two types of linkage of overlapping fault segments in 2D have been identified (Fig. 7), and these are referred to as plane-to-plane and tip-to-plane (following the terminology applied to linkage of joints; Pollard and Aydin, 1988). Plane-to-plane linkage is where a "connecting fault" forms between two overlapping fault segments and bypasses the original fault lobes. The characteristic plane-to-plane fault trace pattern and related displacement profile are shown schematically in Fig. 7A. High displacement gradients within the zone of overlap between the two fault strands reflect the transfer of displacement prior to breaching of the relay zone and steps in the displacement profiles occur at the branch points with the connecting fault. Assuming that movement on the bypassed splays ceased once linkage occurred, the displacement

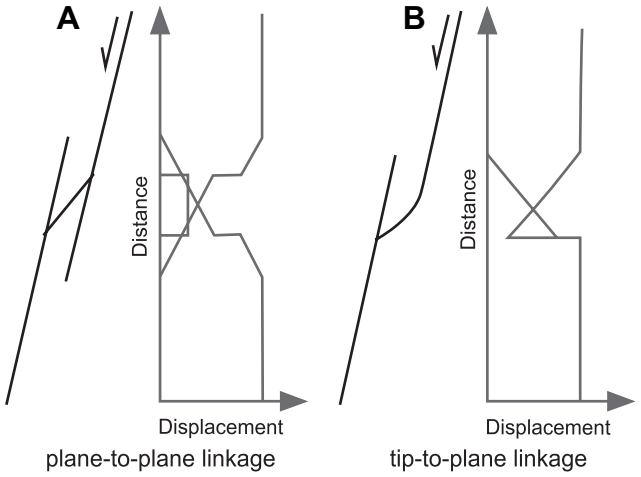

Fig. 7. Schematic illustration of the 2D geometries and displacement profiles of (A) plane-to-plane and (B) tip-to-plane linkage. Fault traces and displacement distributions are shown for relay zones seen in cross-sections of normal faults but the same patterns are associated with neutral relay zones.

at which breaching occurred can be calculated as the difference between the total fault displacement and the displacement on the connecting fault.

Tip-to-plane segment linkage is where one of the segments is deflected towards the other segment to connect with it at a branch point (Fig. 7B). Linkage can occur on either the hanging wall or footwall side and the angle between the two segments at the point of linkage may vary along strike on an individual fault. For the displacement profile shown in Fig. 7B, displacement on the footwall segment decreases towards the branch point and on the hanging wall splay displacement increases towards the branch point. These complementary displacement variations again reflect the transfer of displacement between the initially unconnected fault traces. The step in displacement on the footwall segment records the displacement that accrued after relay breaching. A fault trace pattern similar to that of tip-to-plane linkage could form by back-stepping of a splay into the footwall. In this case, however, the displacement on the footwall segment would be expected to be a maximum at the branch point and decrease upwards in contrast to the displacement distribution shown in Fig. 7B. Although plane-to-plane and tip-to-plane linkages are illustrated for cross-sectional fault traces in Fig. 7, they are also commonly observed in map view (Peacock and Sanderson, 1991, 1994; Childs et al., 1995; Morley and Burhannudinnur, 1997; Peacock and Parfitt, 2002; Soliva and Benedicto, 2004; Hus et al., 2005).

In addition to the two types of linkage, which may occur between overlapping faults, underlapping fault segments (i.e. no overlap between the segments) may coalesce by tip-to-tip linkage. A fault segment boundary bypassed by tip-to-tip linkage is preserved as a bend on the through-going fault trace with an associated displacement low. Identification of sites of tip-to-tip linkage is more ambiguous than linkages between overlapping fault traces; a possible example of tip-to tip linkage was discussed in Section 5.2.

3D examples of plane-to-plane linkage are shown in Fig. 5D (the cross-section at 12.5 cm), and Fig. 8B (the cross-section at 2.5 cm, upper part). The cross-section at 12.5 cm on Fig. 5D has the fault trace pattern and 2D displacement distribution characteristic of plane-to-plane linkage. The throw on the connecting fault is 2 mm and the throw on both bypassed fault strands decreases from 1 mm at the branch point with the connecting fault to zero at the fault tip. If it were assumed that the bypassed splays became inactive when the connecting fault formed, then the low displacement on the bypassed strands relative to the connecting fault would suggest that linkage between the overlapping segments occurred relatively early, when the fault had one-third of its present day throw at this location.

A 2D interpretation of the structure on the 12.5 cm section (Fig. 5D), which considered only fault propagation within the plane of inspection, would conclude that the relay zone was breached by upward or downward propagation of the connecting fault, from one of the two overlapping fault strands, to intersect the second strand. However, in 3D the connecting fault is seen to have its maximum displacement near the point of bifurcation of the two fault-lobes and the displacement decreases towards the overall fault tip-line, i.e. to the left in Fig. 5B. This displacement distribution indicates that the connecting fault propagated from the point of bifurcation, perpendicular to the plane of section and is a lateral extension of the main fault surface rather than a newly formed connecting fault. In addition, the plane-to-plane linkage on the section at 12.5 cm gives way along strike to an intact relay zone (cross-section at 14 cm) between fault segments that were therefore active after linkage occurred on the cross-section at 12.5 cm.

Fig. 8 shows the 3D structure of a portion of a fault close to its upper tip-line. The fault comprises three unconnected fault strands on the cross-section at −1 cm, which give way along strike to a continuous fault strand with two hanging wall splays (cross-section at 4 cm). The intervening cross-sections reveal a complex pattern of fault linkage. Possible 2D interpretations of the structure on the 4 cm cross-section might be progressive back-stepping of the fault into the footwall as it propagated upwards to leave inactive splays in its hanging wall or formation of splays as accommodation structures in the hanging wall of a through-going fault. However, in 3D it is clear that neither of these interpretations is valid as the splays and the main fault diverge along strike to form the bounding faults of two contractional relay zones. We therefore infer that the hanging wall splays on the 4 cm cross-section are tip-to-plane linkages between fault strands that were initially unconnected on this section. The fault surface is continuous to the left of the 4 cm cross-section on Fig. 8A, suggesting that segmentation occurred by bifurcation of the fault surface close to the 4 cm section and that the separate segments diverged as the fault propagated upwards and laterally. The hanging wall splays at 4 cm are short, and their displacements are low, in relation to their along-strike extensions (e.g. cross-section at 0 cm), indicating that breaching of the initial contractional relay zones at these locations occurred at low displacements. We interpret the lower of the two contractional

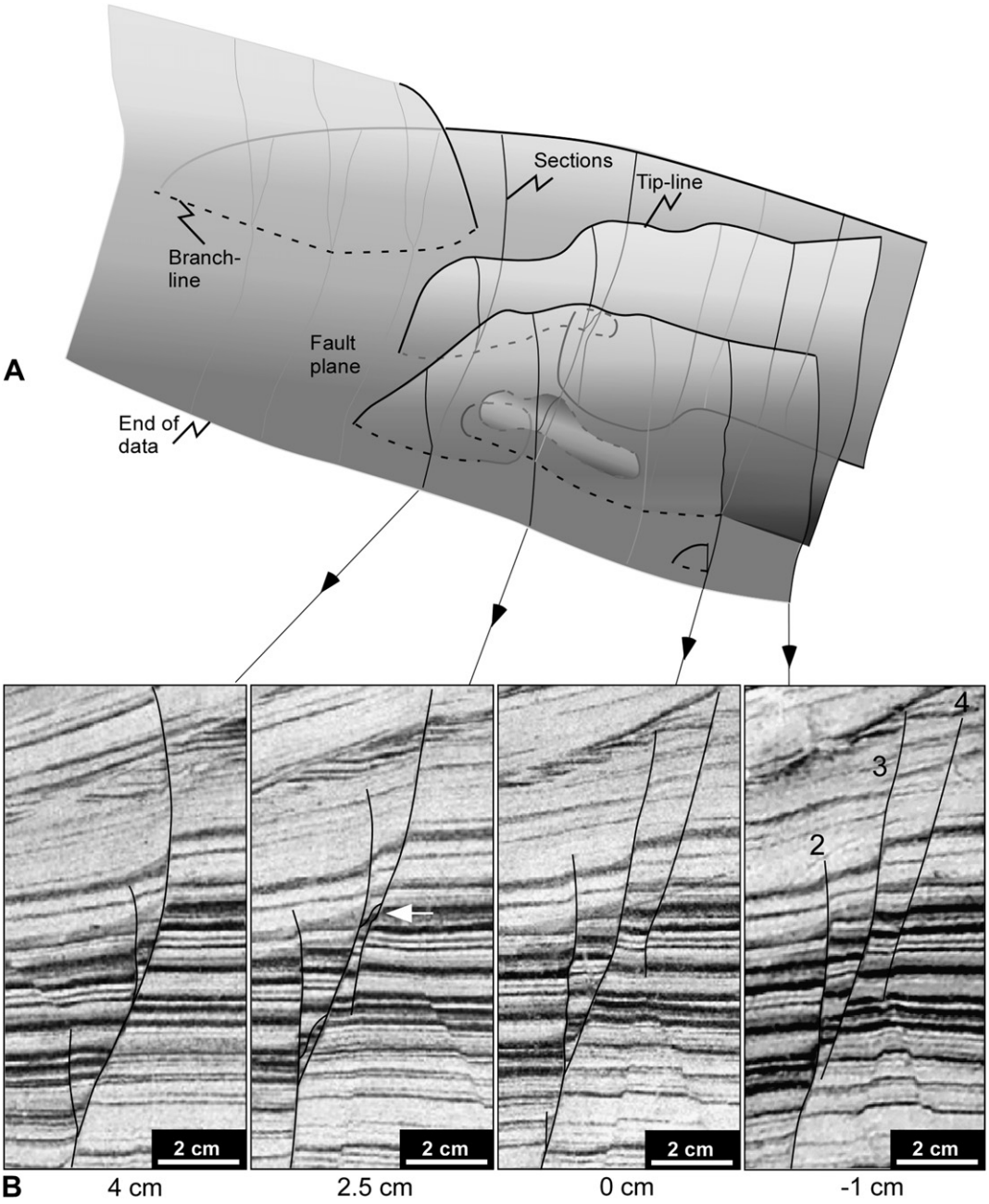

Fig. 8. (A) Map of part of a bifurcated fault surface constructed from 11 cross-sections spaced over a fault strike length of 10 cm; fault geometries on selected cross-sections are shown. Heavy lines denote fault tips (grey where overlapped), branch-lines are shown dashed and unornamented margins of the fault surface are end of data. The figure is exaggerated by a factor of 1.4 in the fault strike direction. (B) Cross-sections at −1.0 cm, 0.0 cm, 2.5 cm and 4.0 cm; the relative locations of the cross-sections are shown in (A). The arrow at 2.5 cm shows the plane-to-plane linkage.

relay zones on the −1 cm cross-section (between Faults 2 and 3) as an example of a relay zone immediately prior to tip-to-plane linkage. An increase in displacement on Fault 3 would result in a downward propagation of its lower fault tip forming a tip-to-plane linkage with Fault 2 and extending the branch-line along which these two segments join. In our model for the evolution of the structure between Faults 2 and 3, therefore, the branch-line along which these faults link developed first at the point of bifurcation of the two fault surfaces (i.e. at the left end of the present day branch-line in Fig. 8A) and extended along strike (towards the right in Fig. 8A) as fault displacement increased. The linkage between Faults 3 and 4 has a tip-to-plane linkage pattern on the 4 cm cross-section and plane-to-plane linkage at 2.5 cm giving way to unlinked segments at 0 cm.

The 3D geometries associated with plane-to-plane and tip-to-plane linkage and our model for their formation are illustrated in Fig. 9. In both cases the breaching structures initiate at the point where the two fault segments first bifurcated. In tip-to-plane linkage, breaching occurs by the propagation of a branch-line from the point of bifurcation (point X in Fig. 9). In plane-to-plane linkage, two branch-lines connecting the linking fault

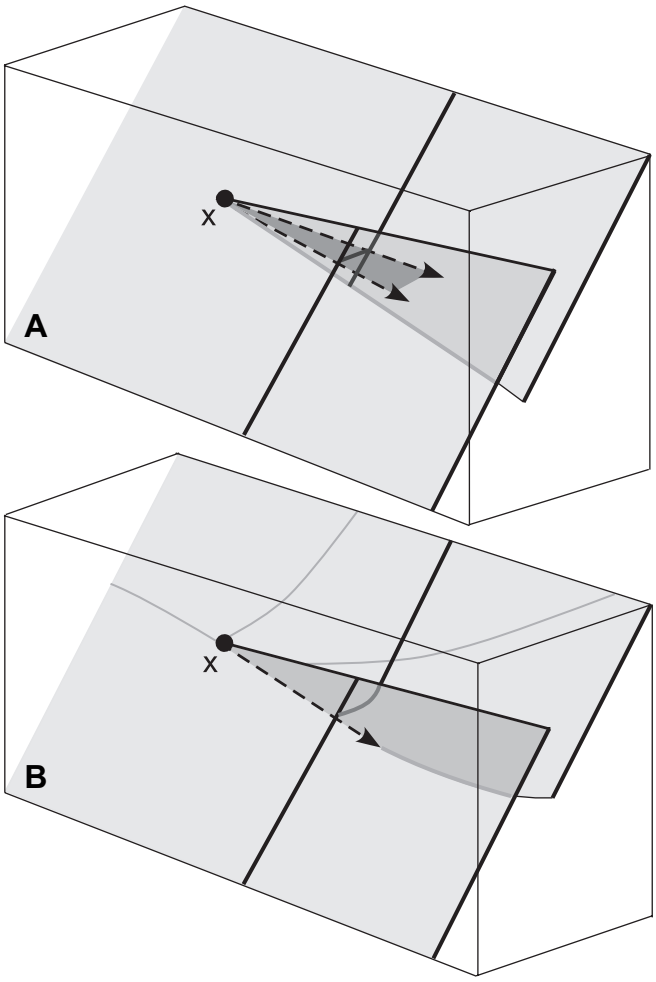

Fig. 9. Schematic illustrations of the 3D geometry associated with plane-to-plane (A) and tip-to-plane (B) breached relay zones. Fault surfaces are shaded with overlapping fault segments shown in darker shading. Heavy black lines show the fault trace geometry on two vertical cross-sections. Branch-lines (dashed lines) are shown with arrowheads indicating the direction in which the branch-line has propagated; to the left of the arrowhead(s) the relay zone is breached and to the right it is intact. In (A) a fault linking the two relay bounding surfaces is shown with dark shading. The solid circle (labelled *X*) is the point of initial bifurcation of the fault surface and the thin lines in (B) are former tip-line locations (see text).

with the two fault segments propagate from the point of bifurcation. In both cases breaching is achieved by propagation of the main fault surface along the axis of the relay zone rather than by the formation of a new breaching fault. Close to the point of bifurcation, where the segment separation is small, relay zone breaching will occur almost immediately after bifurcation, while the two segments continue to propagate along strike to develop a larger separation and longer lived relay structure.

5.4. Stage 4 – lenses

The fourth relay zone growth stage considered in this paper (Fig. 1) involves continued linkage between overlapping fault segments to form a fault bounded lens. The lenses observed in this data set vary from intact lenses bounded by a simple branch-line loop to irregular lens shapes with intense internal faulting. Here we describe two of the simpler structures examined. In the example shown in Fig. 10 a near continuous branch-line loop outlines a sliver of undeformed host sediment. The lens is open at one end where the branch-line gives way to an obliquely plunging tip-line segment (right hand side of Fig. 10) forming the upper boundary of the hanging wall segment. On horizon maps that intersect this tip-line (e.g. Horizon A) the fault pattern is a hanging wall splay connected to the footwall fault at a branch point on the left-hand side in Fig. 10; on maps that do not intersect the tip-line a fault bounded lens is seen. The lateral displacement variations on the lens bounding faults are seen from the geometry of Horizon A. Bedding within the fault bounded sliver dips predominantly to the right in Fig. 10 so that there is a decrease in displacement to the right on the hanging wall fault segment with a complementary increase in displacement on the footwall fault. This map geometry and displacement variation would generally be interpreted as a neutral, map view, relay zone that has been breached at one end. On vertical cross-sections that intersect the tip-line, the fault geometry is an upward divergent hanging wall splay. The throw on the splay decreases rapidly upwards, with displacement transfer onto the through-going footwall fault so that the geometry and displacement distribution at this location are suggestive of tip-to-plane linkage of a contractional relay zone. Our interpretation of this structure is that it initiated as an oblique relay

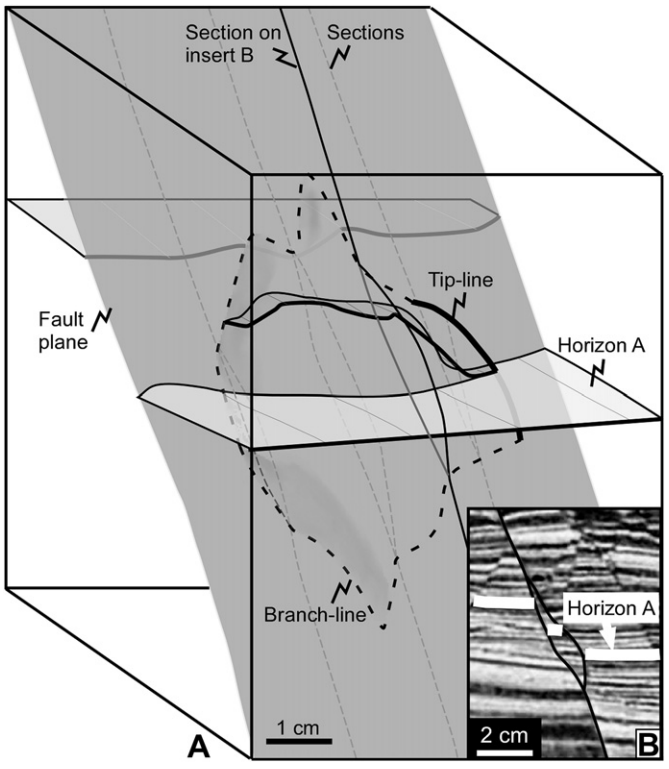

Fig. 10. (A) Fault surface map showing a fault bounded lens constructed from 13 cross-sections, of which the fault traces from four are shown. The branch-line (dashed) is complete apart from the right hand side where there is a short tip-line segment (heavy line). One mapped horizon is shown; Horizon A is shown with light shading. (B) A cross-section (Black in A) through the lens. The horizon shown in (A) is shown white.

zone, demonstrating characteristics of a neutral relay zone or a contractional relay zone, depending on whether the structure is viewed in map view or cross-section, respectively. By analogy with structures described in the previous section we infer that breaching would have initiated at the point of fault bifurcation but there is insufficient evidence on which to speculate where this point is on the present day branch-line. We would expect that with further increase in displacement the branch-line would form a continuous loop.

Fig. 11A shows a 3D fault surface map of a lens with a more irregular geometry than the previous example. The lens is again open at one end so that on cross-sections towards the centre of the structure the lens geometry is apparent (cross-section at 2.5 cm), while to the right (e.g. the cross-section at 0 cm) the structure is seen as a hanging wall splay. On the left-hand side of Fig. 11A (cross-section at 4 cm) there is an upwardly diverging splay on the hanging wall side of the lens presumed to be a relict of the hanging wall bounding fault of an original contractional relay zone at this location. The interpretation of this lens as a breached contractional relay zone is also consistent with the presence of the hanging wall splay on the 0 cm cross-section and also with the displacement distribution on the lens bounding faults (Fig. 11C). Once again, maps through this structure which intersect the upper tip-line of the hanging wall splay on the right hand side of Fig. 11A will have the fault pattern associated with breaching of a neutral, map view relay zone, and lateral displacement variations on a particular horizon would support this interpretation (compare the throws at X and X' on Fig. 11B). Unlike the previous example (Fig. 10) in which the fault throw was comparable on the two lens bounding faults, in this structure the throw on the footwall fault is significantly higher than that on the hanging wall fault. This asymmetry may indicate that the lens is bypassed by the footwall fault and will not evolve further with increased displacement.

6. The structure of a fault array

In the previous sections we described individual examples of segment boundaries that are together interpreted to demonstrate growth stages from fault surface bifurcation through to the formation of a fault bounded lens. Here we describe the geometry and displacement transfer of a single fault array as illustrated in Figs 12 and 13; the structure of three of the segments within this array was described previously (Faults 2, 3 and 4; Fig. 8). On a vertical cross-section the fault array (Fig. 12A) comprises four fault segments (Faults 1–4), three of which are linked in the plane of section, while the fourth is linked along strike (Fig. 8). The aggregate throw profile for the fault array (Fig. 12B) shows a regular upward decrease in throw towards the upper tip-point, with transfer of displacement between adjacent segments so that the different fault segments are elements of a geometrically coherent array (Walsh and Watterson, 1991). A similar pattern of fault displacements is seen in map view. Fig. 12D shows structure maps for four mapped horizons (highlighted in Fig. 12A) and on these the fault system comprises a series of predominantly right stepping segments. Transfer of displacement between adjacent segments is shown by high lateral displacement gradients (Fig. 12C) and high bed dips in the areas of overlap between segments (Fig. 12D). The boundaries between the fault segments in Fig. 12 show relay zone characteristics in both map view and cross-section and are oblique relay zones. The fault array is therefore a system of fault segments that bifurcated during propagation to form a series of oblique relay zones that are preserved at various stages of breaching.

In addition to Faults 1–4, there are fault segments in the footwall to this array, Faults 5 and 6, which although not connected to the main array on Fig. 12A, do link along strike, again displaying complementary displacement variations indicating that these are also components of this fault array on a larger scale.

The fault array illustrated in Fig. 12 is simplified and not all of its geometrical complexities are shown. Fig. 13, however, shows a map of the branch-lines and tip-lines for all of the mapped fault segments within this fault array. This map highlights not only the complexity of structure associated with this fault array, but also the variability in this complexity over the fault surface; an area of complex fault structure (i.e. with displacement distributed on multiple anastomosing and rejoining splays) gives way along strike to a portion of the fault where there is a single continuous planar fault surface. The controls on the numbers of segments formed at different points on this and other faults within our data sets are not well understood. A strong lithological control on segmentation would be reflected in a predominantly vertical variation in the degree of fault segmentation yet the numbers of segments do not appear to vary with elevation on the fault. We tentatively conclude that the primary control on fault segmentation is spatial variation in the stress field into which the fault surface propagated due, for example, to movement on nearby faults.

Part of the overall tip-line of the fault array in Fig. 13 is mapped within the data volume and indicates that the mapped array is the upper left-hand portion of a larger structure. In addition, the point of maximum cumulative displacement on the mapped fault array is on the lower right of Fig. 13 (see displacement profiles in Fig. 12A, C) suggesting that the mapped part of the fault array formed by propagation upwards and towards the left. It is clear from Fig. 13 that the minor structural elements within the fault array do not have any simple relationship with the inferred propagation direction. It might be expected, for example, that the preserved tip-lines of faults bounding relay zones would radiate from the point of maximum displacement of the fault surface, i.e. the lower right in Fig. 13. Similarly, it might be expected that segment boundaries or fault bounded lenses would be elongate parallel to, or normal to, the propagation direction. No such simple patterns are observed and both the shapes and orientations of segment boundaries are highly variable. The only systematic aspect of the fault segments on this fault array is that they are more likely to have branch-lines on their lower boundaries and tip-lines on their upper boundaries than *vice versa*. We suggest a model, illustrated in Fig. 9B, to explain this observation. An upward propagating fault tip-line becomes pinned

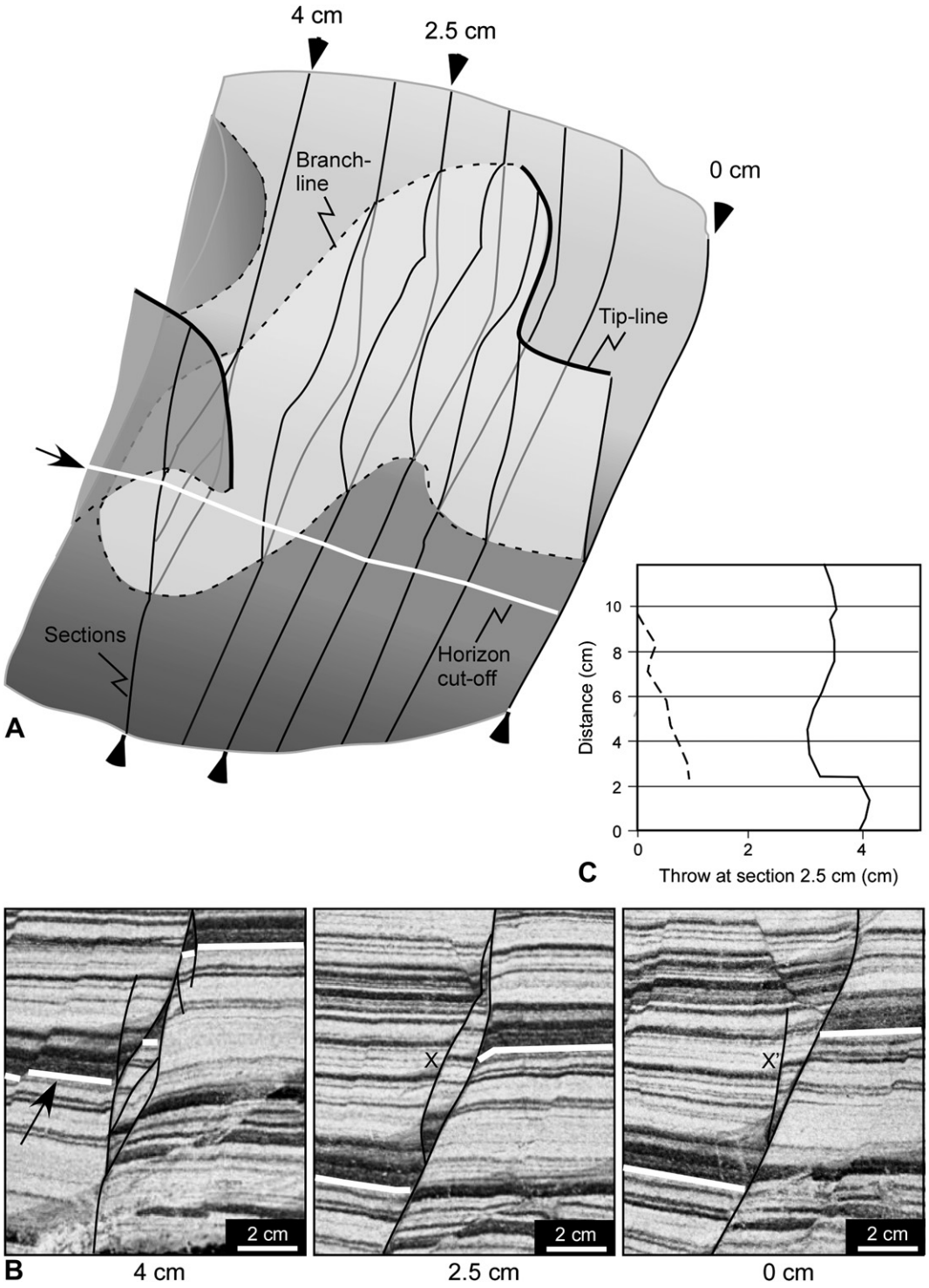

Fig. 11. (A) Oblique view of part of a fault surface with an open lens (light shading), constructed from fault trace geometries recorded on 8 cross-sections (shown on the fault surface). The branch-line (dashed) is complete, apart from the right hand side where there is a tip-line segment (heavy line). The arrow and white line on the figure show the elevation of the hanging wall cutoff of the horizon arrowed in (B). The figure is exaggerated by a factor of 1.4 in the fault strike direction. (B) Three cross-sections are shown at distances of 0.0 cm, 2.5 cm and 4.0 cm along fault strike; the relative locations of the cross-sections are shown in (A). (C) Throw profiles for the traces of the hanging wall (dashed line) and footwall (solid line) faults on the cross-section at 2.5 cm.

along the part of its length to the right of the point labelled *X* in Fig. 9B. The tip-line to the left of *X* is free to continue propagating and a series of tip-line locations through time are shown as the new fault lobe propagates into the footwall of the pinned fault, eventually establishing a relay zone. Because the tip-line section to the right of *X* is pinned then the relay zone must be breached by downward propagation of the upper lobe, so that the newly formed branch-line develops at the lower boundary of the relay zone. This model would predict that fault splays will more frequently diverge away from,

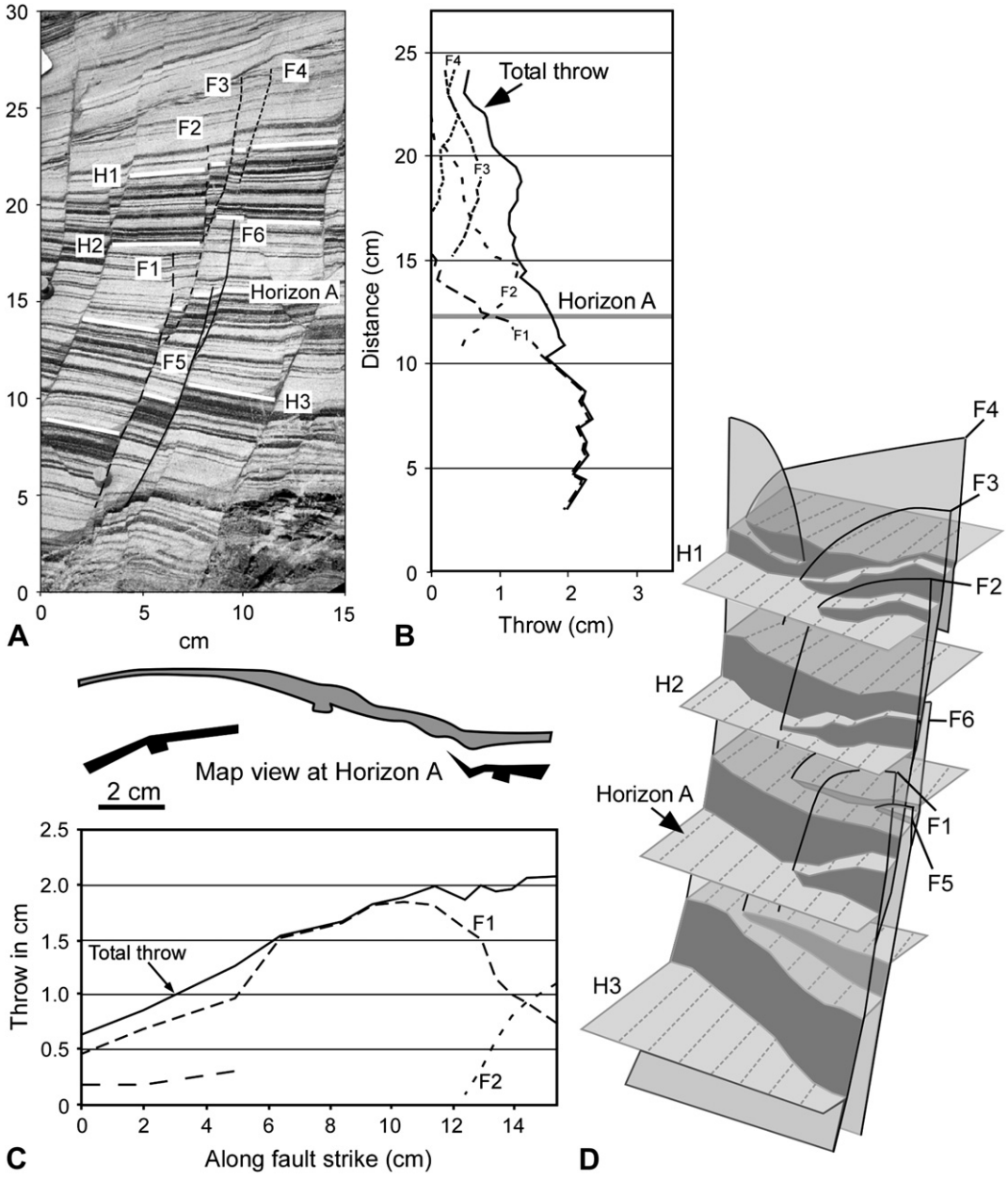

Fig. 12. (A) Cross-section of fault splays interpreted with dotted lines and numbered 1–4 from left to right. Horizons are denoted H1–H3 and Horizon A. (B) Throw profiles for the fault splays shown in (A) and their aggregate throw summed on a horizon by horizon basis. (C) Along-strike throw profile for Faults 1 and 2 and a third related fault, together with their aggregate throw, for Horizon A highlighted in (A) and (B). (D) Oblique view of the fault array. Fault tip-lines (heavy lines) and the four horizons marked in white (H1–H3 and Horizon A) on the cross-section in (A) are shown. Lines on the horizon surfaces are the intersection lines with the nine cross-sections used to construct the figure. The nine sections shown occur between along fault strike distance 8 and 15 cm on (C). For the sake of clarity branch-lines are not drawn on the diagram.

rather than towards, the point of maximum displacement on a fault trace.

7. Discussion

In this paper we have studied the geometries of small faults in soft sediments. The advantage of this type of study is that, due to the low fault displacements and high displacement gradients, entire faults or significant parts of faults can be contained within a relatively small volume of sediment. Although the faults studied are small, we expect that the geometries recorded would also be seen on large faults if appropriate data were available. Where detailed 3D data on fault geometry are available for large faults, structures similar to those described here have been recognised. For example, the various stages of evolution of neutral relay zones have been recognised for large faults from high quality seismic reflection data (Walsh et al., 1999; Marchal et al., 2003). Huggins et al. (1995) recorded, from mine plans of stacked coal seams, a neutral relay zone that formed a gap on an otherwise continuous fault surface on a fault with a displacement of 3 m; the mapped 3D geometry is similar to that shown in Fig. 6A.

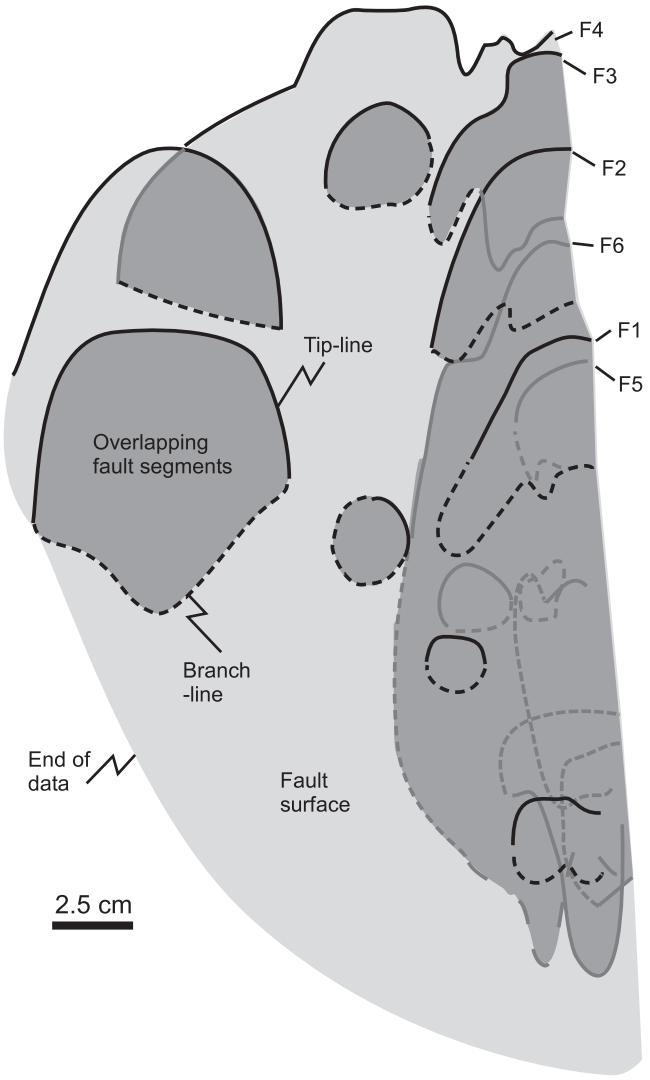

Fig. 13. Diagram showing the outlines of fault segments within the fault array presented in Fig. 12, projected onto a vertical plane parallel to fault strike. Here the branch-lines (dashed) are shown along with the tip-lines (full lines, grey in the footwall). Dark areas show areas of overlap of one or more fault segments. The lower and right hand edges of the figure are end of data.

These, and other, previous studies have been concerned primarily with describing the evolution of neutral relay zones, largely because recognition of contractional and extensional relay zones from 3D seismic data are frequently ambiguous (but see examples in Walsh et al., 1999 and Kattenhorn and Pollard, 2001). Therefore, although many of the 3D geometries of contractional and extensional relay zones described here have not been previously described, this is attributable to a lack of appropriate data, and we expect that similar geometries to those we have described will occur for faults of all sizes. Similarly the geometries recorded here are not limited to faults in soft sediments and the cross-sectional geometries observed here are readily observed in 2D sections of small faults in a range of lithologies (e.g. Peacock and Zhang, 1993; Childs et al., 1996a; Burhannudinnur and Morley, 1997; van der Zee and Urai, 2005). The detailed characteristics of 3D fault geometry are, however, expected to vary from one lithology/sequence to another. For example, in sequences with a significant mechanical contrast between layers, faults are expected to initiate first in the competent layers with subsequent linkage through weak layers (Eisenstadt and De Paor, 1987; Childs et al., 1996a; Peacock, 2002). In this case fault segment boundaries will occur preferentially at weak layers and would be elongate parallel to bedding. In mechanically isotropic, but stronger rocks than the sediments studied here, e.g. massive, cemented sandstones, the strains which could be accommodated by deformation within a relay zone prior to breaching would be low compared to those recorded here making it difficult to demonstrate the presence of pre-existing relay zones.

Our data suggest that embayments in the tip-line of a propagating fault surface are common and that fault surfaces, when viewed in sufficient detail, are fringed by numerous overlapping lobes rather than by simple tip-line loops. Fig. 13 illustrates the very complicated propagation pathways, which may occur as a fault grows. The portion of the enveloping fault tip-line that is contained within the data volume is a simple curve. However, the variability in the orientations of tip-lines that bound fault segments demonstrates that locally propagation may occur in any direction as individual fault lobes expand. This complexity in the 3D structure of fault arrays should be considered when devising models for fault evolution from 2D data.

8. Conclusions

1. Serial sections through faults in soft sediment illustrate the very complex internal structure of faults. Areas where a fault comprises a single slip surface alternate with areas with multiple anastamosing surfaces.
2. The 3D geometry of selected fault segment boundaries demonstrate a previously proposed four-stage model for their evolution involving (1) fault surface bifurcation, (2) relay zone formation, (3) relay zone breaching, and (4) lens formation.
3. Contractional and extensional relay zones may occur as ‘holes’ within an otherwise continuous fault surface.
4. Relay zone breaching initiates at the point of bifurcation of fault segments, as the parent fault surface propagates along the axis of the relay zone, so that the relay zone may be intact and breached at different points along its length.

Acknowledgements

This work was funded by EU INFAMI Project No: NNE5-2000-20087, Contract No: ENK6-CT2000-00072. The authors would like to thank the partners on the INFAMI project. All members of Fault Analysis Group at University College Dublin are thanked for helpful discussions. Peter Bretan at Badleys Geoscience is thanked for helpful, friendly and timely support using TrapTester5.2. Thanks to Chris Bonson for reading an early version of the manuscript. Jonathan Imber and David Peacock are thanked for their useful reviews of the manuscript.

References

Burhannudinnur, M., Morley, C.K., 1997. Anatomy of growth faults zones in poorly lithified sandstones and shales: implications for reservoir studies and seismic interpretation: part 1, outcrop study. Petroleum Geoscience 3, 211–224.

Cartwright, J.A., Trudgill, B.D., Mansfield, C.S., 1995. Fault growth by segment linkage; an explanation for scatter in maximum displacement and trace length data from the Canyonlands Grabens of SE Utah. Journal of Structural Geology 17, 1319–1326.

Childs, C., Watterson, J., Walsh, J.J., 1995. Fault overlap zones within developing normal fault systems. Journal of the Geological Society, London 152, 535–549.

Childs, C., Nicol, A., Walsh, J.J., Watterson, J., 1996a. Growth of vertically segmented normal faults. Journal of Structural Geology 18, 1389–1397.

Childs, C., Watterson, J., Walsh, J.J., 1996b. A model for the structure and development of fault zones. Journal of the Geological Society, London 153, 337–340.

Childs, C., Walsh, J.J., Watterson, J., 1997. Complexity in fault zone structure and implications for fault seal prediction. In: Møller-Pederson, P., Koestler, A.G. (Eds.), Hydrocarbon Seals: Importance for Exploration and Production. NPF Special Publication, vol. 7. Elsevier, Singapore, pp. 61–72.

Eisenstadt, G., De Paor, D.G., 1987. Alternative model of thrust-fault propagation. Geology 15, 630–633.

Huggins, P., Watterson, J., Walsh, J.J., Childs, C., 1995. Relay zone geometry and displacement transfer between normal faults recorded in coal-mine plans. Journal of Structural Geology 17, 1741–1755.

Hus, R., Acocella, V., Funiciello, R., De Batist, M., 2005. Sandbox models of relay ramp structure and evolution. Journal of Structural Geology 27, 459–473.

Kattenhorn, S.A., Pollard, D.D., 2001. Integrating 3-D seismic data, field analogs, and mechanical models in the analysis of segmented normal faults in the Wytch Farm Oil Field, Southern England, United Kingdom. AAPG Bulletin 85, 1183–1210.

Kristensen, M.B., 2005. Soft Sediment Faulting – Investigation of the 3D Geometry and Fault Zone Properties. Aarhus Geoscience, Ph.D. thesis 25.

Larsen, P.-H., 1988. Relay structures in Lower Permian basement-involved extension system, East Greenland. Journal of Structural Geology 10, 3–8.

Mansfield, C., Cartwright, J., 2001. Fault growth by linkage: observations and implications from analogue models. Journal of Structural Geology 23, 745–763.

Marchal, D., Guiraud, M., Rives, T., Van den Driessche, J., 1998. Space and time propagation processes of normal faults. In: Jones, G., Fisher, Q.J., Knipe, R.J. (Eds.), Faulting, Fault Sealing, and Fluid Flow in Hydrocarbon Reservoirs. Geological Society, London, Special Publications, vol. 147, pp. 51–70.

Marchal, D., Guiraud, M., Rives, T., 2003. Geometric and morphological evolution of normal fault planes and traces from 2D to 4D data. Journal of Structural Geology 25, 135–158.

Morley, C.K., Burhannudinnur, M., 1997. Anatomy of growth fault zones in poorly lithified sandstones and shales: implications for reservoir studies and seismic interpretation: part 2, seismic reflection geometrics. Petroleum Geoscience 3, 225–231.

Peacock, D.C.P., Sanderson, D.J., 1991. Displacements, segment linkage and relay ramps in normal fault zones. Journal of Structural Geology 13, 721–733.

Peacock, D.C.P., Zhang, X., 1993. Field examples and numerical modelling of oversteps and bends along normal faults in cross-section. Tectonophysics 234, 147–167.

Peacock, D.C.P., Sanderson, D.J., 1994. Geometry and development of relay ramps in normal fault systems. AAPG Bulletin 78, 147–165.

Peacock, D.C.P., 2002. Propagation, interaction and linkage in normal fault systems. Earth-Science Reviews 58, 121–142.

Peacock, D.C.P., Parfitt, E.A., 2002. Active relay ramps and normal fault propagation on Kilauea Volcano, Hawaii. Journal of Structural Geology 24, 729–742.

Pollard, D.D., Aydin, A., 1988. Progress in understanding jointing over the past century. Geological Society of America Bulletin 100, 1181–1204.

Ramsay, J.G., Huber, M.I., 1983. The Techniques of Modern Structural Geology. Academic press.

Rasmussen, E.S., Dybkjær, K., 2005. Sequence stratigraphy of the Upper Oligocene-Lower Miocene of eastern Jylland, Denmark: role of structural relief and variable sediment supply in controlling sequence development. Sedimentology 52, 25–63.

Rowan, M.G., Hart, B.S., Nelson, S., Flemings, P.B., Trudgill, B.D., 1998. Three-dimensional geometry and evolution of a salt-related growth-fault array: Eugene Island 330 field, offshore Louisiana, Gulf of Mexico. Marine and Petroleum Geology 15, 309–328.

Soliva, R., Benedicto, A., 2004. A linkage criterion for segmented normal faults. Journal of Structural Geology 26, 2251–2267.

van der Zee, W., Urai, J.L., 2005. Processes of normal fault evolution in a siliciclastic sequence: a case study from Miri, Sarawak, Malaysia. Journal of Structural Geology 27, 2281–2300.

Walsh, J.J., Watterson, J., 1991. Geometric and kinematic coherence and scale effects in normal fault systems. In: Roberts, A.M., Yielding, G., Freeman, B. (Eds.), The Geometry of Normal Faults. Geological Society Special Publications, vol. 56, pp. 193–203.

Walsh, J.J., Watterson, J., Bailey, W.R., Childs, C., 1999. Fault relays, bends and branch-lines. Journal of Structural Geology 21, 1019–1026.

Walsh, J.J., Bailey, W.R., Childs, C., Nicol, A., Bonson, C.G., 2003. Formation of segmented normal faults: a 3-D perspective. Journal of Structural Geology 25, 1251–1262.

Wibberley, C.A.J., Petit, J.P., Rives, T., 1999. Mechanics of high displacement gradient faulting prior to lithification. Journal of Structural Geology 21, 251–257.